City Research Online

City, University of London Institutional Repository

A New Design of Cable Anchor for Ultra-High Fatigue Stress Cable Net of Largest Telescope in the World

Wanxu Zhu[1], Kefei Jia[2], Feng Fu[3], Dongqiu Lan[4], Kai Qian[5]

Abstract

As the largest filled-aperture radio telescope in the world, China's five-hundred-meter diameter Aperture Spherical Radio Telescope (FAST) is supported using a unique ultra-high fatigue stress cable net structure to enable flexible deformation of the reflector. As each of the supporting cables is required to be capable of bearing an ultra-high fatigue stress (up to approximately 500 MPa), a new type of cable anchor is specially designed in this paper to provide required high prestress level in the cables. In this paper, the stress distribution of the steel strands inside the chilled cast anchor is analyzed, a method for adjusting the prestress force of the cable anchor is developed which can effectively reduce the stress concentration of the steel strands inside chilled cast anchor. The relationship between the anchorage efficiency coefficient and its influencing factors is established, which can be used for the design of the anchor and to optimize the performance of cable anchorage.

Keywords: FAST Project; Cable Anchor; Stress; Fatigue Design; Stress Concentration.

---

[1]Wanxu Zhu. Professor, College of Civil Engineering and Architecture, Guilin University of Technology, Guilin, 541004, China. E-mail: zhuwanxu@vip.163.com

[2]Kefei Jia. Lecturer, College of Civil Engineering and Architecture, Guilin University of Technology, Guilin, 541004, China. E-mail: jaakefei@gmail.com

[3]Feng Fu, Senior Lecturer, School of Mathematics, Computer Science & Engineering, City, University of London, EC1V, 0HB, London, Professor, College of Civil Engineering and Architecture, Guilin University of Technology, Guilin, 541004, China. E-mail: cenffu@yahoo.co.uk

[4]Dongqiu Lan, Research Student, College of Civil Engineering and Architecture, Guangxi University, Nanning, 530001, China. E-mail: gxtm_2018@st.gxu.edu.cn

[5]Kai Qian, Professor, College of Civil Engineering and Architecture, Guilin University of Technology, Guilin, 541004, China. E-mail: qiankai@gxu.edu.cn (Corresponding author)

1. Introduction

As the largest single caliber radio telescope and the most sensitive spherical radio telescope in the world [1] (as shown in Fig. 1), China's Five-hundred-meter Aperture Spherical Radio Telescope (FAST) has helped scientists to discover 51 pulsar candidates since its trial operation in September 2016, 11 of which have been officially confirmed as new pulsars [2]. FAST's reflector can deform actively to generate a 300-meter-diameter instantaneous parabolic antenna to capture the electromagnetic waves emitted from the object under observation [3-5].

Fig. 1. FAST project
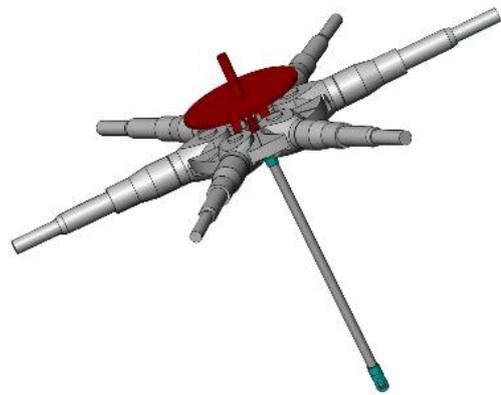
Fig. 2. Cable joints in FAST project

As FAST's reflector is anticipated to complete over 1,000,000 times of active deformation in its first 30 years of operation, it is important to equip it with a specially designed supporting system to support the highly demanding operation [6-7]. Starting from 1994, the National Astronomical Observatories of China (NAOC) together with many universities and research institutes had conducted feasibility studies of various supporting systems before finally deciding on the cable net structure [8-9] (Fig. 2). Taking into account the fact that the cables of the cable net supporting system will be subject to fatigue at an ultra-high stress amplitude up to 470 MPa during the long-term operation, it is required that the cables have an infinite fatigue life at 500 MPa stress level [10-14].

In comparison, according to current standards [15-17], it is usually required that cable failure be avoided at a stress amplitude of merely 200 MPa with a maximum stress of $0.4\sigma_b$ (where σ_b is the standard strength), or, in the cases of a few bridges, at 250 MPa with a maximum stress of $0.45\sigma_b$

[18-20]. Wang et al. [21] designed a chilled cast anchor for stay cables, it is capable of resisting bear over 2 million load cycles with a stress amplitude of 200 MPa. Feng et al. [22] proposed a high-capacity anchorage system for multitendon carbon fiber-reinforced polymer (CFRP) cables and the associated construction technology. The cable anchorage system sustained 2 million cycles without any macroscopic cracks forming in either the cable or anchorage at a maximum stress of 0.45fs (the standard strength value) and a stress range of 200 MPa. Ping et al. [23] developed an innovative bonded anchor with steel wedges at the free end. it is capable of resisting bear over 2million load cycles with a stress amplitude of 161 MPa. Thus, the existing cables need to be improved to meet the requirement of 500 MPa fatigue stress level.

The performance of cable anchor affects the fatigue resistance of cables [24]. Due to its outstanding fatigue resistance, chilled cast anchor was u in the FAST project. However, the existing chilled cast anchor was unable to meet the requirement of 500 MPa fatigue stress amplitude [25]. Besides the defects of the material itself, the main reason is the serious stress concentration in cable anchor developed during the working state. The influence of stress concentration on structural performance is closely related to the loading mode of the structure. Compared with static load or quasi-static load, when the structure is subjected to cyclic load, the damage accumulation is faster at the position of stress concentration, so the structure will fail faster. Stress concentration is a key factor affecting the performance of cable anchor. Reducing stress concentration can improve the fatigue resistance of cable anchor effectively [26-27].

This research aims to reduce the stress concentration and optimize the fatigue resistance of cable anchor by adjusting the stress distribution inside the chilled cast anchor. The stress distribution of the steel strands inside the chilled cast anchor is analyzed, a method of the stress adjustment is developed, and the relationship between the anchorage efficiency coefficient and its influencing factors is identified.

Finally, a double-cone cable anchor is proposed with enhanced design, which enables the cables to meet the aforementioned high standards, and its stress distribution is analyzed.

2. Stress Analysis of Chilled Cast Anchor

2.1 Mechanisms

The structure of a chilled cast anchor filled with epoxy iron sand is shown in Fig. 3. The process of steel strands being prestressed in the anchor cup can be divided into two phases.
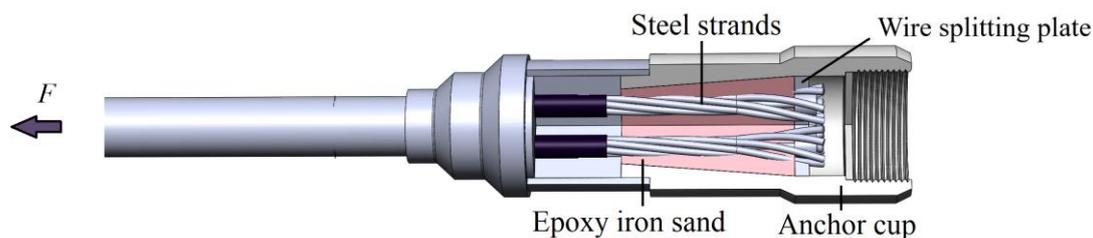
Fig. 3. Schematic diagram of the chilled cast anchor

Phase I: As shown in Fig. 3, when the steel strands are under tension force F, it stretches, thus driving the wire splitting plate to move in the same direction, forcing the epoxy iron sand to move into the anchor cup. As a result of the wedge effect of the anchor cup, the epoxy iron sand is continuously compressed. The above situation will make epoxy iron sand wrap the steel strands more vigorously. In other words, the radial pressure on the steel strands from the epoxy iron sand will increase gradually, and the friction force of steel strands from epoxy iron sand will also increase gradually. In this phase, steel strands will slip from the epoxy iron sand continuously.

Phase II: In phase I, steel strands will slip from the epoxy iron sand continuously, but this sliding is not unlimited. The friction force of steel strands from epoxy iron sand will increase gradually. When the friction force is equal to the tension force F, steel strands stop slipping from the epoxy iron sand. With the increase of the tensile force F, steel strands together with the epoxy iron sand continue to stay compressed, causing the radial pressure of the steel strands and epoxy iron sand to increase. As a result,

the epoxy iron sand is in full contact and matching tightly with the steel strands until a final stable grip is achieved.

In most cases, before put to operation, a cable must be pre-tensioned with a tensile force larger than what the cable will undergo in actual working conditions to eliminate the Phase I slippage between the steel strands and the epoxy iron sand, and also to ensure a fixed cable length and better fatigue performance.

2.2. Internal Stress Calculation
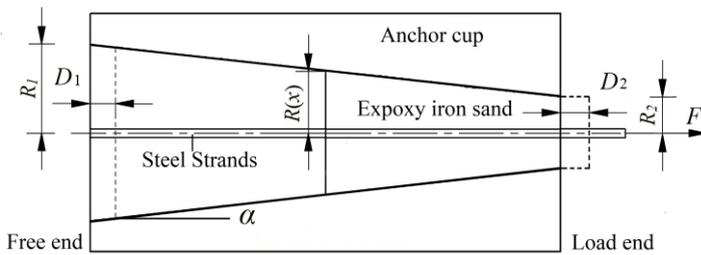
Fig. 4. Calculating diagram of the chilled cast anchor   **Fig. 5.** Cross section
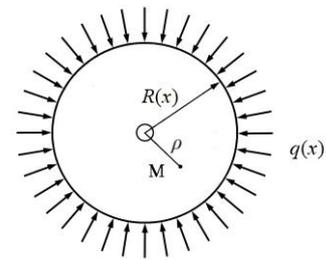
Based on basic rules of Elasticity, the anchor cup is divided, along the steel strands, into n sections equal in length and the following assumptions are made: 1) The epoxy iron sand is fully compact; 2) The cable anchor (including the steel strands and the epoxy iron sand) is homogeneous and elastic; 3) Ignoring radial deformation of anchor cup; 4) Ignoring the influence of shear-lag effect, each section is always plane.

When an tensile force F is applied to the cable anchor, the steel strands and the epoxy iron sand will slip from the anchor cup as shown in Fig. 4 where the dotted lines indicate the position after the slippage; α is the inner inclination angle of the anchor cup; R_1 and R_2 are the radius of the free end and that of the load end, respectively; D_1 and D_2 are the axial displacement of the free end and that of the load end, respectively. In Fig. 5, an examined cross section is analyzed, where x is the distance from the

cross section to the free end; $R(x)$ is the radius of the cross section; $q(x)$ is the radial stress. The radial displacement of the cross section is provided in the equation.

$$u(x) = -D(x)\tan\alpha \tag{1}$$

where $u(x)$ is the radial displacement of the cross section; $D(x)$ is the axial displacement of the cross section.

The assumption is made that the cross section is a thick-walled cylinder with a negligible inner diameter. Therefore, in Fig.5, According to Eq. (45) in the appendix, for point M, the following equation is true

$$\sigma_\rho(x,\rho) = -q(x) \tag{2}$$

According to Eq. (47) (shown in Appendix), the radial displacement of M (i.e., the radial displacement of the cross section) can be calculated as follows:

$$u(x) = -\frac{1-v-2v^2}{E}q(x)R(x) = -\frac{1-v-2v^2}{E}q(x)(R_1 - x\tan\alpha) \tag{3}$$

where v is the Poisson ratio; E is the elastic modulus.

According to Eq. (1), the axial displacement of M can be calculated as follows:

$$D(x) = \frac{(R_1 - x\tan\alpha)(1-v-2v^2)}{E\tan\alpha}q(x) \tag{4}$$

It is assumed that the epoxy iron sand moves in the anchor cup but the length remains unchanged, i.e., $D(x)$ is assumed to be a constant. The radial stress of the free end and that of the load end are q_1 and q_2, respectively, and the radial stress distribution diagram is drawn based on Eq. (4).
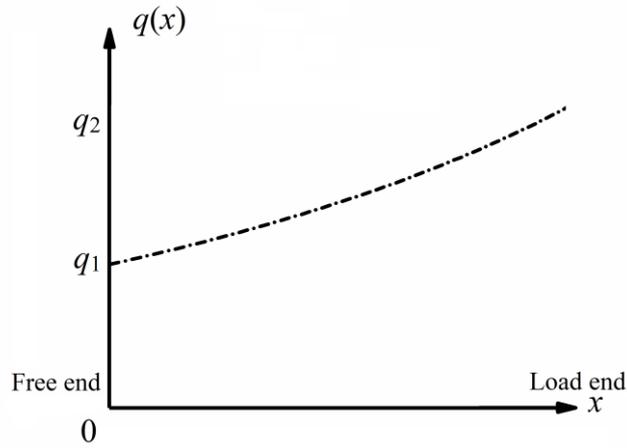
Fig. 6. Radial stress distribution diagram along the whole length

As shown in Fig. 6, the radial stress of the epoxy iron sand increases from q_1 to q_2 along the axial direction as the distance to the free end increases, and the non-linear correlation is observed. With the axial deformation of the epoxy iron sand taken into account, the closer the cross section to the load end, the greater the deformation. Therefore, $D_2 > D_1$, and q_2 is consequently much larger than q_1. The radial stress distribution at the interface between the epoxy iron sand and the anchor cup (first interface) is shown in Fig. 7, and the radial stress distribution at the interface between the steel strands and the epoxy iron sand (second interface) is shown in Fig. 8. According to Fig. 8, the radial stress of the steel strands is not evenly distributed. To be specific, at the load end, the steel strands bear the largest radial compressive stress as well as the largest axial tensile stress. Therefore, stress concentrates at this location, making it a weak spot of the entire cable anchor. The material properties of the steel strands largely remain untapped due to severe stress concentration at the load end, making it difficult for the cable net to meet the fatigue requirements at ultra-high stress amplitude as mentioned. The key to an optimum design is to lower the compressive stress level of steel strands at the load end.
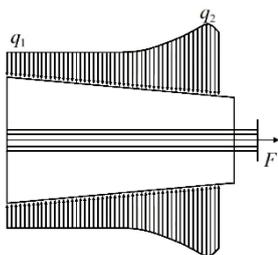
Fig. 7. Radial stress distribution at the first
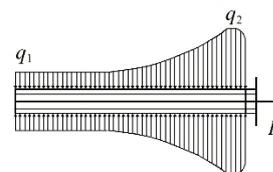
Fig. 8. Radial stress distribution at the second

7

3. Parameters Affecting Cable Anchor Performance

There are basic requirements for cable anchor, including: 1) sufficient self-anchoring with anchorage efficiency coefficient that matches the standards; 2) No sliding of steel strands from the epoxy iron sand.
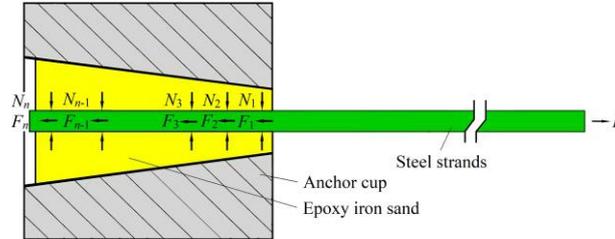
Fig. 9. Calculating diagram of the cable anchor

In below analysis, the anchor cable anchor is divided into n micro- segments with equal length along the steel strands as shown in Fig. 9, where N_i is the radial compressive force from the epoxy iron sand onto the ith segment ($i = 1, 2, ..., n$) of the steel strands; F_i is the frictional force from the epoxy iron sand onto the ith segment of the steel strands. Vectors are excluded to simplify the analysis.

3.1 Friction Coefficient and Inner Inclination Angle of Anchor Cup

To avoid loosening during the transportation and installation processes, the cable anchor must be self-anchoring. In other words, after epoxy iron sand is squeezed into the anchor cup, it will not be retracted back; therefore, the following requirement must be met:

$$\alpha < \beta \tag{5}$$

where α is the inner inclination angle (i.e., the taper angle of the outer surface of the epoxy iron sand); β is the friction angle of the outer surface of the epoxy iron sand. In most cases, α is approximately equal to 5°, and β is approximately equal to 7°.

To ensure zero slippage between the epoxy iron sand and the steel strands, a radial compressive force must be applied to the epoxy iron sand. When the steel strands and the epoxy iron sand are

considered as one integrated unit, the following equations can be obtained according to the force balance:

$$\sum_{i=1}^{n} F_i = F = \sum_{i=1}^{n} P_i \tan(\alpha + \beta) = \frac{2\pi H \tan(\alpha + \beta)}{n} \sum_{i=1}^{n} q_i r_i \tag{6}$$

where P_i is the radial compressive force exerted on the outer surface of the ith segment of the epoxy iron sand; q_i is the radial stress on the outer surface of the ith segment; r_i is the outer radius of the ith segment; H is the total length of the epoxy iron sand; n is the total number of micro-segments.

In another case where the epoxy iron sand and the steel strands are considered as two separate components, to ensure no sliding of the steel strands from the epoxy iron sand, the following must be true:

$$F \leq \mu \sum_{i=1}^{n} N_i \tag{7}$$

where μ is the equivalent friction coefficient between the steel strands and the epoxy iron sand.

Considering the possibility of the epoxy resin aging, the bond between the steel strands and the epoxy iron sand is excluded from the analysis, therefore:

$$\frac{2\pi H \tan(\alpha + \beta)}{n} \sum_{i=1}^{n} q_i r_i \leq \frac{\mu \pi d H}{n} \sum_{i=1}^{n} \sigma_i \tag{8}$$

where d is the equivalent radius of the steel strands; σ_i is the radial stress of the steel strands of the ith segment.

According to Eq. (2), $\sigma_i = q_i$; so

$$\mu \geq \frac{2r_i}{d} \tan(\alpha + \beta) \tag{9}$$

To ensure zero slippage, replace r_i with R_1; so

$$\mu \geq \frac{2R_1}{d} \tan(\alpha + \beta) \tag{10}$$

9

where it can be seen that the larger the inner diameter of the free end of the anchor cup is, the more likely the steel strands are to slide. Therefore, small values of R_1 will be favorable for improved cable anchor performance.

3.2 Factors Influencing Anchorage Efficiency Coefficient

For every segment of the steel strands, the first principal stress σ_1 is approximately equivalent to the axial tensile stress, and the third principal stress σ_3 is approximately equivalent to the radial compressive stress. Taking into account the stress concentration of the axial tensile stress and the radial compressive stress due to factors such as the heterogeneity of the epoxy iron sand materials, the following equations are obtained:

$$\sigma_1 = k_{i1}\bar{\sigma}_{1i}; \sigma_3 = k_{i3}\bar{\sigma}_{3i} \tag{11}$$

where $\bar{\sigma}_{1i}$ is the average axial tensile stress of the ith segment; $\bar{\sigma}_{3i}$ is the average radial compressive stress of the ith segment; k_{i1} is the stress concentration coefficient of the axial tensile stress of the ith segment; and k_{i3} is the stress concentration coefficient of the radial compressive stress of the ith segment.

Generally speaking, all segments share the same value of the stress concentration factor; therefore, k_1 and k_3 are used to represent the stress concentration coefficients of the axial tensile stress and the radial compressive stress, respectively. According to material mechanics, $\sigma_1 - \sigma_3 < \sigma_b$. Thus, the following is obtained:

$$k_1\bar{\sigma}_{1i} - k_3\bar{\sigma}_{3i} \leq \sigma_b \tag{12}$$

where σ_b is the standard strength of the steel strands.

As for the ith segment of the steel strands, according to material mechanics, the average axial stress of steel strands is shown as

$$\bar{\sigma}_{1i} = \frac{F}{S_i} - \sum_{j=1}^{i-1} \frac{F_j}{S_i} \tag{13}$$

10

where S_i is the cross-sectional area of the ith segment of the steel strands.

For different segments of the steel strands, the interface friction between the epoxy iron sand and the steel strands mostly remains constant. Therefore, it is assumed that, regarding the steel strands, the radial compressive force N_i is proportionally correlated with the axial frictional force F_i in all segments, which is described as

$$F_i = kN_i \tag{14}$$

where k is the ratio of the radial compressive force to the axial frictional force, $k \leq \mu$. Assuming the reduction in cross-sectional area due to compression from the epoxy iron sand is negligible, the following is true:

$$S_i = S \tag{15}$$

where S is the cross-sectional area of the steel strands.

Drawing on Eq. (12) and Eq. (13), we have

$$\sum_{i=1}^{n} k_1 \bar{\sigma}_{1i} S_i - \sum_{i=1}^{n} k_3 \bar{\sigma}_{3i} S_i \leq n\sigma_b S \tag{16}$$

$$k_3' = \frac{dn}{4H} k_3 \tag{17}$$

$$k_1 \sum_{i=1}^{n} (F - \sum_{j=1}^{i-1} F_j) - k_3' \sum_{i=1}^{n} N_i \leq nF_b \tag{18}$$

$$k_1 (nF - \sum_{i=1}^{n} \sum_{j=1}^{i-1} F_j) - k_3' \sum_{i=1}^{n} N_i \leq nF_b \tag{19}$$

where F_b is the standard ultimate tensile force of the steel strands. Also, we have

$$\begin{aligned}
&\sum_{i=1}^{n} \sum_{j=1}^{i-1} F_j \\
&= (n-1)F_1 + (n-2)F_2 + (n-3)F_3 + \ldots + 2F_{n-2} + F_{n-1} \\
&= \frac{n-1}{2} F_1 + (\frac{n-2}{2} F_2 + \frac{1}{2} F_1) + (\frac{n-3}{2} F_3 + \frac{1}{2} F_2 + \frac{1}{2} F_1) + \ldots + \sum_{i=1}^{n-1} \frac{1}{2} F_i \\
&= k[\frac{n-1}{2} N_1 + (\frac{n-2}{2} N_2 + \frac{1}{2} N_1) + (\frac{n-3}{2} N_3 + \frac{1}{2} N_2 + \frac{1}{2} N_1) + \ldots + \sum_{i=1}^{n-1} \frac{1}{2} N_i]
\end{aligned} \tag{20}$$

$$\sum_{i=1}^{n} \sum_{j=1}^{i-1} F_j \leq k[\frac{n-1}{2} N_1 + (\frac{n-2}{2} N_2 + \frac{1}{2} N_2) + (\frac{n-3}{2} N_3 + \frac{1}{2} N_3 + \frac{1}{2} N_3) + \ldots + \frac{n-1}{2} N_n] \tag{21}$$

11

$$\sum_{i=1}^{n}\sum_{j=1}^{i-1}F_j \le \frac{n-1}{2}k\sum_{i=1}^{n}N_i \tag{22}$$

$$\sum_{i=1}^{n}\sum_{j=1}^{i-1}F_j \le \frac{n-1}{2}F \tag{23}$$

Based on the results from the above calculations, the following is obtained:

$$k_1(n-\frac{n-1}{2})F + k_3'\frac{F}{k} \le nF_b \tag{24}$$

As n approaches infinity, the following is true:

$$\frac{F}{F_b} \le \frac{4}{2k_1+\dfrac{d}{Hk}k_3} \tag{25}$$

when F reaches the ultimate tensile force of the steel strands (F_{pk}), the following is obtained:

$$\frac{F_{pk}}{F_b} \le \frac{4}{2k_1+\dfrac{d}{Hk}k_3} \tag{26}$$

The anchorage efficiency coefficient is defined as η_A, $\eta_A = F_{pk}/F_b$, so

$$\eta_A \le \frac{4}{2k_1+\dfrac{d}{Hk}k_3} \tag{27}$$

$K \le \mu$, so

$$\eta_A \le \frac{4}{2k_1+\dfrac{d}{H\mu}k_3} \tag{28}$$

when Eq. (10) is substituted into Eq. (30), the following is obtained:

$$\eta_A \le \frac{2}{k_1+k_3\dfrac{S}{\pi HR_1\tan(\alpha+\beta)}} \tag{29}$$

m_A is defined as the anchorage efficiency index; so

$$m_A = \frac{2}{k_1+k_3\dfrac{S}{\pi HR_1 \tan(\alpha+\beta)}} \tag{30}$$

Based on the above analyses, the following conclusions are made:

12

1) The larger the anchorage performance efficiency index (m_A) is, the greater the anchorage efficiency coefficient (η_A) can be. Eq. (30) shows how to optimize the cable anchor without affecting the performance.

2) The smaller the stress concentration coefficients (k_1 and k_3) are, the larger η_A will be. Given that k_1 and k_3 are largely dependent on the elastic modulus and the degree of uniformity of the epoxy iron sand, measures can be taken accordingly to optimize anchorage efficiency.

3) As can be inferred from Eq. (30), the longer the epoxy iron sand (H), the higher the anchorage efficiency coefficient.

4) η_A increases as the inner diameter of the anchor cup at the free end (R_1) or the sum of the taper angle (α) and the friction angle (β) increases, on the condition that there is no slippage.

5) If α is lowered to improve the self-anchoring performance, it is necessary to increase β or H to keep k_1 and k_3 from increasing.

6) In engineering practice, due to the structural size constraints, it is still very difficult to achieve an even distribution of stress; the load end usually features stress concentration. Therefore, steel strands tend to break at the load end of the anchor cup when reaching the ultimate tensile force or receiving fatigue damage.

4. A new type Cable anchor

4.1 Optimization Design
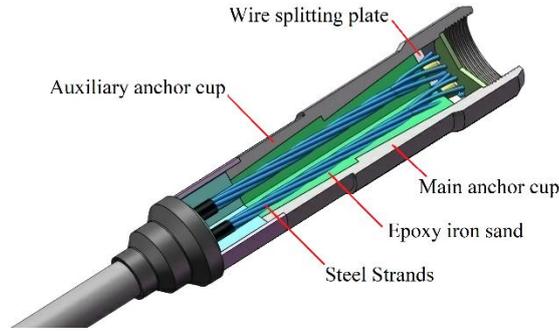
Fig. 10. Schematic diagram of double-cone cable anchor

Based on the analyses presented above, a new double-cone cable anchor including a main anchor cup and an auxiliary one is developed, as shown in Fig. 10. The inner inclination angle of the main anchor cup is larger than that of the auxiliary anchor cup, which ensures larger frictional force from the anchor cup onto the epoxy iron sand at the main anchor cup than at the auxiliary cup. As a result, the stress concentration at the load end is significantly reduced, the material properties of the steel strands are fully taken advantage of and the fatigue resistance of the cable anchor is thus improved. With the steel strands being connected to the wire splitting plate, the steel wire is dispersed. This method increases the friction coefficient between the epoxy iron sand and the steel strands, lowering the likelihood of slipping under ultra-high stress amplitude.

4.2 Stress Analysis of Double-cone Cable Anchor
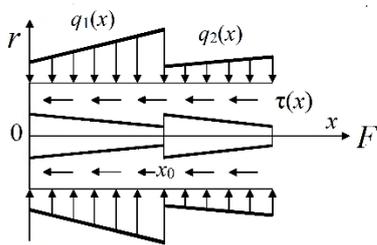
Fig. 11. Stress distribution of the epoxy iron sand
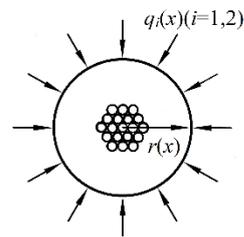
Fig. 12. Cross section

The internal stress distribution of the double-cone cable anchor is shown in Fig. 11and Fig. 12, where $q_1(x)$ and $q_2(x)$ are the radial stress of the epoxy iron sand at the main anchor cup and that at the

auxiliary anchor cup, respectively; $\tau(x)$ is the stress at the interface between the epoxy iron sand and steel strands.

The calculation diagram of double-cone cable anchor is shown in fig. 13.
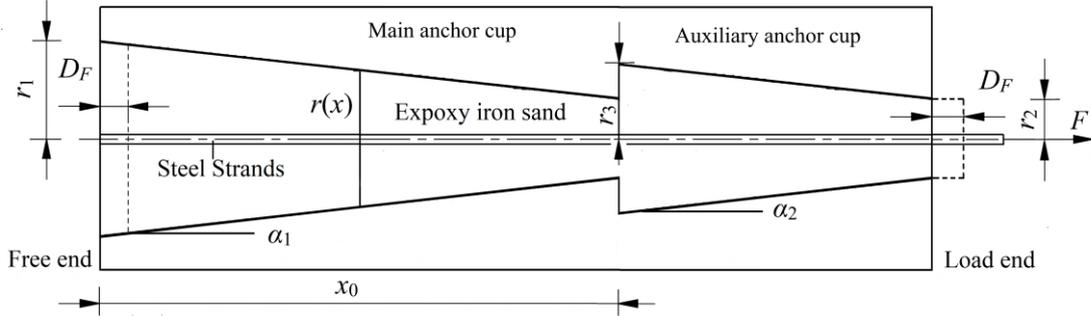
Fig. 13. Calculation diagram of double-cone cable anchor

The following equations can be obtained according to Eq. (1):

$$u(x) = -D_F \tan \alpha_1 ; (x < x_0) \tag{31}$$

$$u(x) = -D_F \tan \alpha_2 ; (x \geq x_0) \tag{32}$$

where D_F is the axial displacement of any cross section of the epoxy iron sand (all cross sections are assumed to be identical along the axial direction); α_1 is the inner inclination angle of the main anchor cup; α_2 is the inner inclination angle of the auxiliary anchor cup; and x_0 is the length of the main anchor cup.

The following equations can be obtained according to Eq. (3):

$$q_1(x) = \frac{\tan \alpha_1}{\frac{1 - v - 2v^2}{E} (r_1 - x \tan \alpha_1)} D_F \tag{33}$$

$$q_2(x) = \frac{\tan \alpha_2}{\frac{1 - v - 2v^2}{E} [r_3 - (x - x_0) \tan \alpha_2]} D_F \tag{34}$$

where r_1 is the free end radius of the main anchor cup, and r_3 is the free end radius of the auxiliary anchor cup.

15

As shown in the equations above, when the inner inclination angle of the auxiliary anchor cup is smaller than that of the main anchor cup, the compressive stress is relatively small at load end of the auxiliary anchor cup. By setting up an appropriate angle, the stress concentration of steel strands in the cable anchor can be reduced.

According to the elastic mechanics, the radial compressive stress of the steel strands is equal to the radial compressive stress of the epoxy iron sand.

The resultant force (F_1) between the compressive stress of epoxy iron sand and the friction force from anchor cup in the x-axis($x < x_0$) is shown as

$$F_1 = \int_0^{x_0} q_1(x) \cdot 2\pi(r_1 - x\tan\alpha_1)\sin\alpha_1 dx + \int_0^{x_0} q_1(x) \cdot 2\pi(r_1 - x\tan\alpha_1)\tan\beta\cos\alpha_1 dx \tag{35}$$

$$F_1 = \frac{2\pi E x_0 \tan\alpha_1}{1 - v - 2v^2}(\sin\alpha_1 + \tan\beta\cos\alpha_1)D_F \tag{36}$$

The resultant force (F_2) between the compressive stress of epoxy iron sand and the friction force from anchor cup in the x-axis ($x \geq x_0$) is shown as

$$F_2 = \int_{x_0}^{H} q_2(x) \cdot 2\pi[r_3 - (x - x_0)\tan\alpha_2]\sin\alpha_2 dx + \int_{x_0}^{H} q_2(x) \cdot 2\pi[r_3 - (x - x_0)\tan\alpha_2]\tan\beta\cos\alpha_2 dx \tag{37}$$

$$F_2 = \frac{2\pi E(H - x_0)\tan\alpha_2}{1 - v - 2v^2}(\sin\alpha_2 + \tan\beta\cos\alpha_2)D_F \tag{38}$$

The external tensile force F of the cable anchor is the sum of F_1 and F_2; thus:

$$F = \frac{2\pi E}{1 - v - 2v^2}[x_0\tan\alpha_1(\sin\alpha_1 + \tan\beta\cos\alpha_1) + (H - x_0)\tan\alpha_2(\sin\alpha_2 + \tan\beta\cos\alpha_2)]D_F \tag{39}$$

According to Eq. (39), D_F can be obtained. Based on the results, the compressive stress of the epoxy iron sand can be obtained as well. Alternatively, the friction angle β can be obtained by experimentally determining. If $x_0 = 0$, the above formula can be regarded as the calculation formula of a single-cone cable anchor.

The typical S3-cable of the FAST project was taken as an example where $E = 36000$ MPa, $\beta = 5.7°$, $\alpha_1 = 4.1°$, $\alpha_2 = 3°$, $r_1 = r_3 = 33$ mm, $x_0 = 106$ mm, $H = 225$ mm, $v = 0.3$, the maximum design value of the cable force = 312,480 N (40% of the cable force limit, to be safe)[28]. With these parameters, D_F

was calculated as 0.32 mm. By putting this D_F value into Eq. (33) and Eq. (34), the compressive stress at the load end of the main anchor cup and that at the load end of the auxiliary anchor cup were calculated to be 62.49 MPa and 43.37 MPa, respectively.

In the case of a single-cone cable anchor, D_F was calculated as 0.55 mm following the above calculating procedure, and the compressive stress at the load end of the anchor cup was 108.03 MPa, 72.94% larger than that in the case of the double-cone structure. If the single-cone cable anchor is the same in total anchorage length as the double-cone and $\alpha = 4.1°$, then $D_F = 0.26$ mm, and the compressive stress at the load end is 76.63 MPa, which is still larger than that in the case of the double-cone structure; also, comparing to the double-cone, the single-cone design will lead to an increase of the outer diameter of the anchor cup by nearly 20%, which is unfavorable. As can be seen in the comparison, the double-cone effectively adjusts the stress within the anchor cup and keep the size of the anchor cup at a smaller level.

4.3 Finite Element Analysis

The typical S3-cable of the FAST project was taken as an example. In order to compare the stress distribution in the cable anchor before and after optimization, the finite element analysis was carried out. Along the axis of anchorage, 3 symmetrical planes can be constructed, and the anchorage can be divided into 3 identical parts. Therefore, the 1/3 model of the anchorage can meet the requirements of the finite element analysis. The models of 3 kinds of anchors are established respectively, as shown in fig. 14. The material of anchor cup and wire splitting plate is 40Cr, which is isotropic, elastic modulus is 210 GPa and Poisson's ratio is 0.3; The elastic modulus of epoxy iron sand is 36 GPa and Poisson's ratio is 0.3; Ignoring the effect of steel stranded wire twisting, it is simplified as a steel wire with a diameter of 15.4mm. Its elastic modulus is 195GPa, Poisson's ratio is 0.3, yield stress is 1635.3MPa and standard

strength is 1860MPa. The friction coefficient between epoxy iron sand and tendon is 0.3, and that
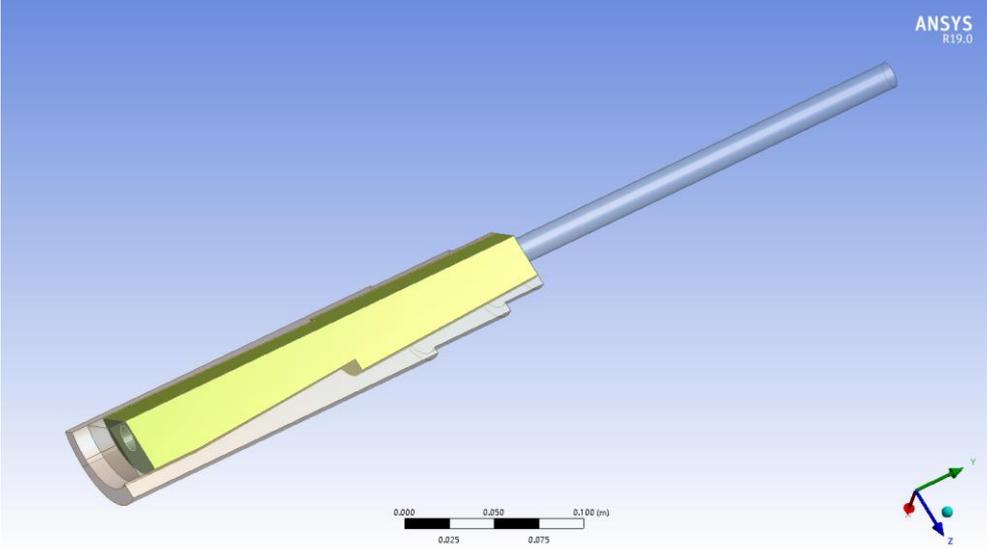
a. Double-cone anchor
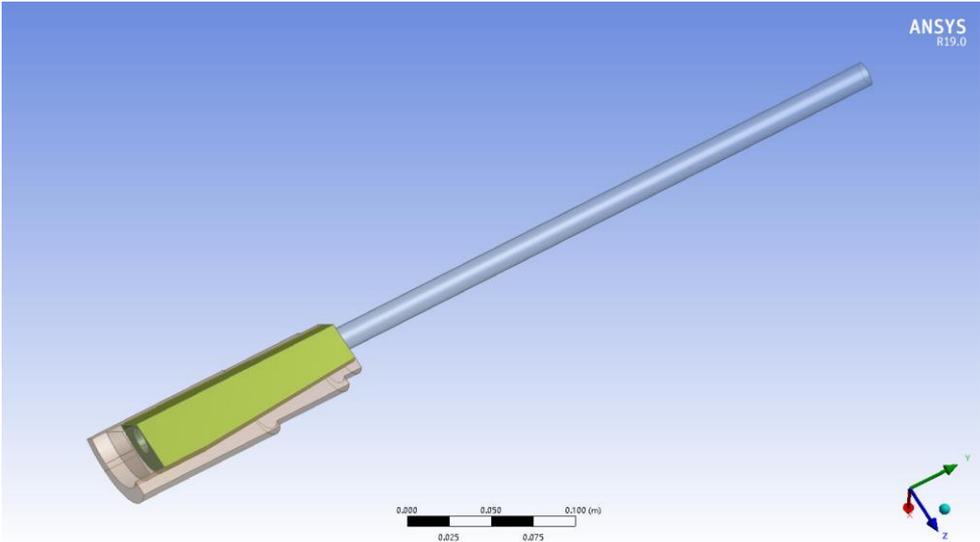
b. Single-cone anchor

between epoxy iron sand and anchor cup is 0.1[28].
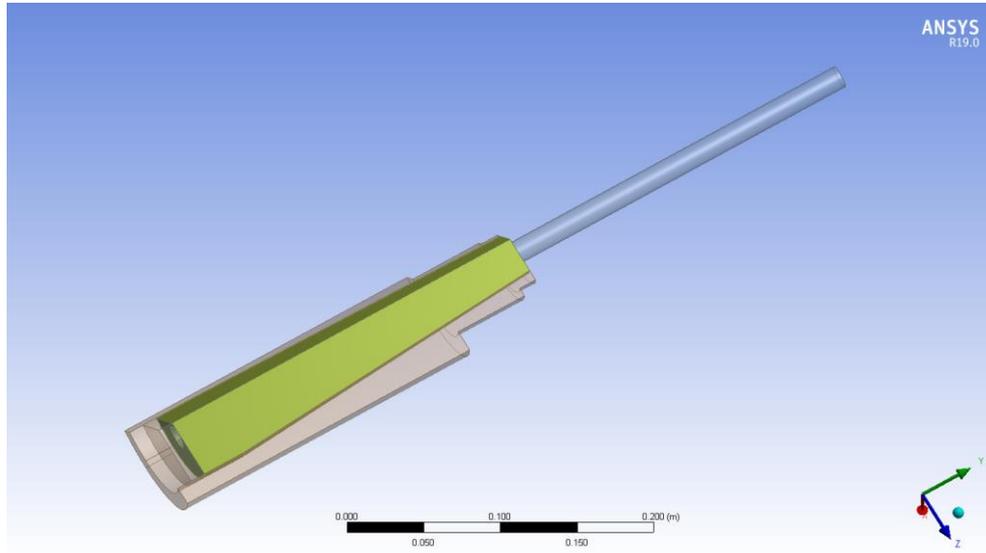
c. Extended single-cone anchor
Fig. 14. Finite element analysis model

a. Double-cone anchor. This kind of anchor is the optimized one. The length of the main anchor cup is 106mm, and the inclination angle is 4.1°; the length of the auxiliary anchor cup is 119mm and the inclination angle is 3°. The total length of the anchor cup is 225mm, and the inner diameter of the anchor cup at the free end is 33mm [28].

b. Single-cone anchor. It is equivalent to removing the auxiliary anchor cup of double-cone anchor. The total length of the anchor cup is 106mm, the inclination angle is 4.1° and the inner diameter of the anchor cup at the free end is 33mm.

c. Extended single-cone anchor. It is equivalent to removing the auxiliary anchor cup of double-cone anchor and increasing the total length of the anchor cup from 106mm to 225mm, the inclination angle is 4.1° and the inner diameter of the anchor cup at the free end is 41.5mm.

The mesh model is shown in Fig.15. Since the purpose of the finite element analysis is to observe the stress concentration on the surface of the steel strands, there are more dense grids on the steel strands than on other components.

19
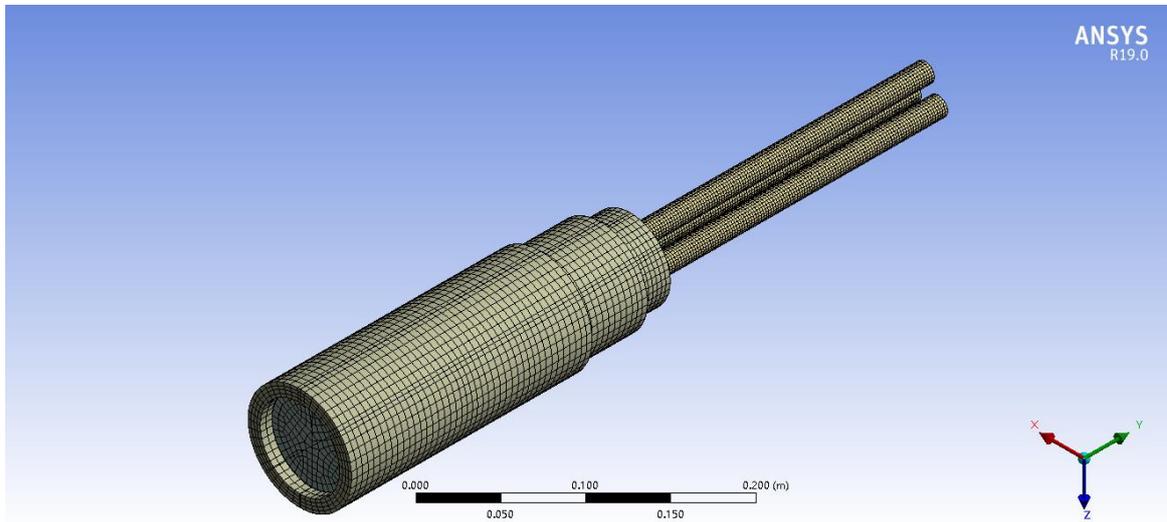
a. Double-cone anchor
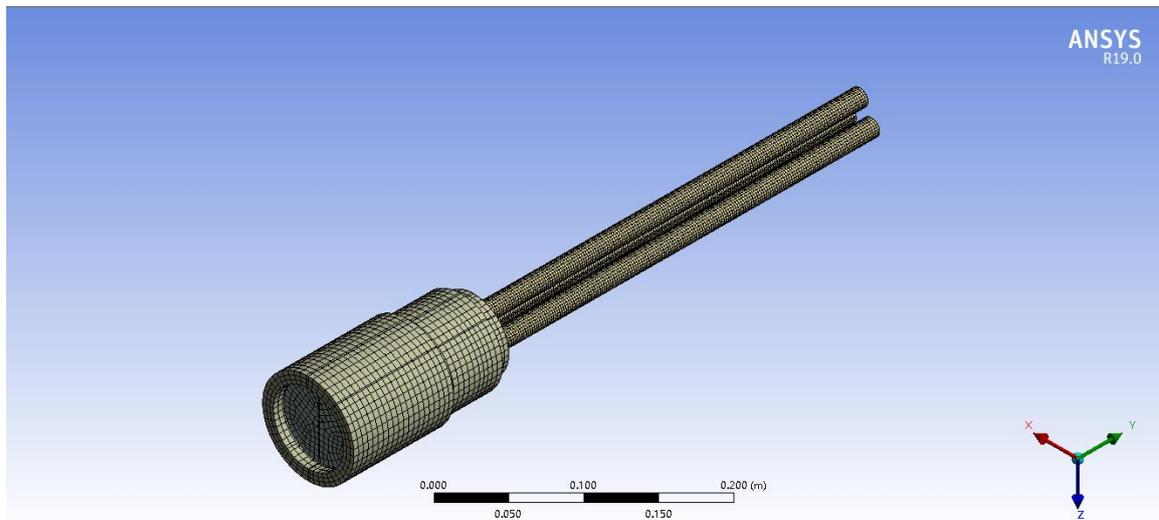
b. Single-cone anchor
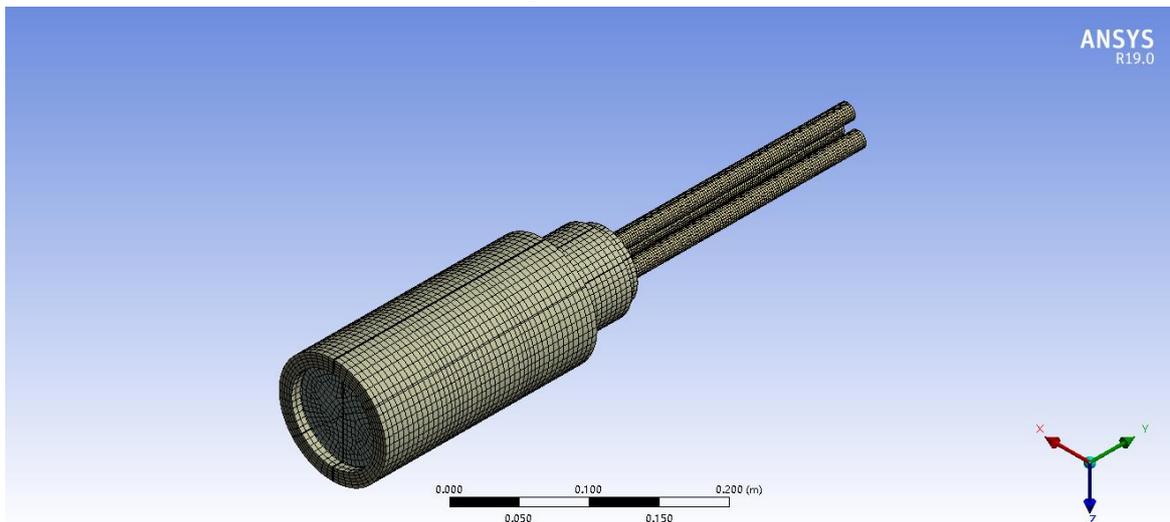
c. Extended single-cone anchor
Fig. 15. Meshing

The uniform stress of 744 MPa ($0.4\sigma_b$, where σ_b is the standard strength) in Y direction was applied to the steel strands, and the displacement of anchor cup in Y direction was restrained. The Mises stress distribution on the steel strands is shown in fig. 16.
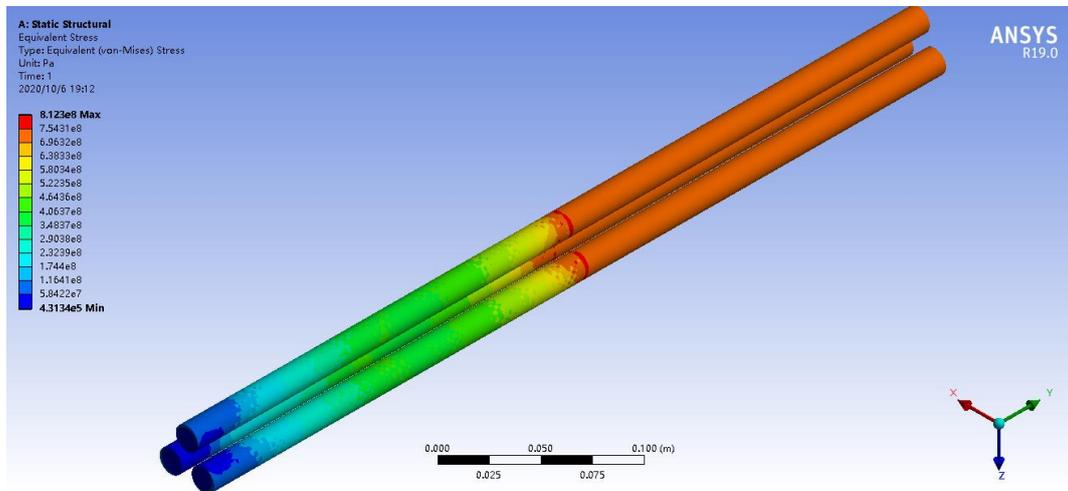
a. Double-cone anchor
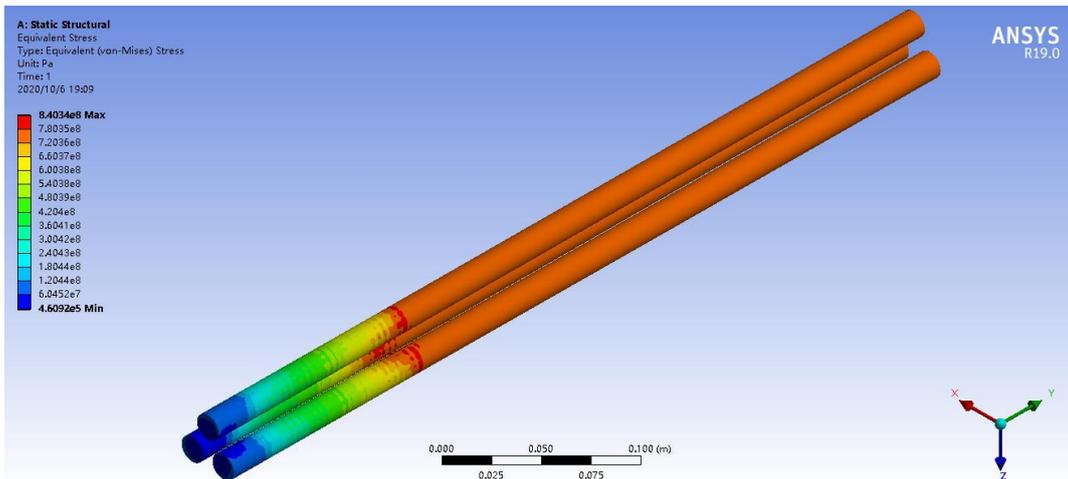
b. Single-cone anchor
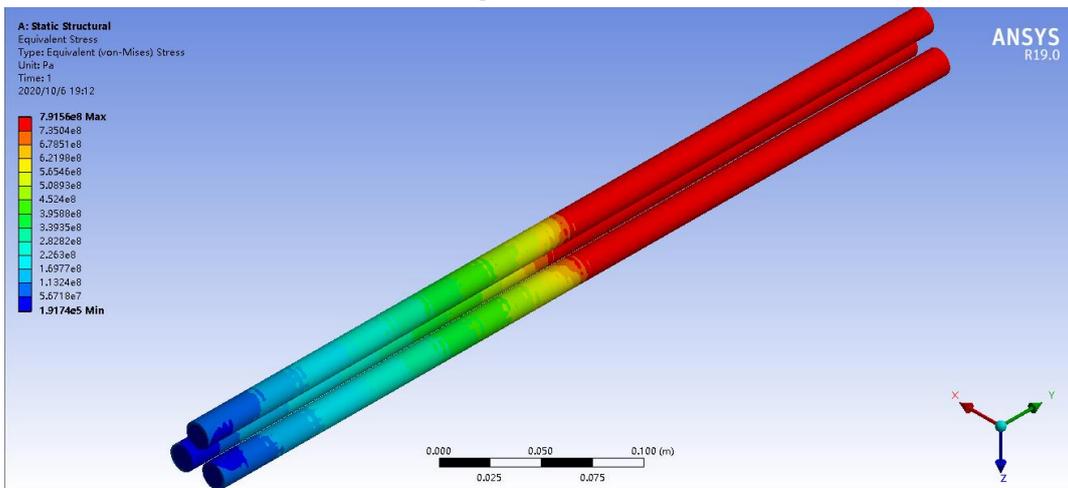
c. Extended single-cone anchor
Fig. 16. The Mises stress distribution on the steel strands

The results of finite element calculation are summarized in Table 1.

Table 1

The results of finite element calculation

Model	Maximum Mises stress (MPa)	Tensile stress (MPa)	Ratio (%)
Double-cone anchor	812.3	744	109.2
Single-cone anchor	840.3	744	112.9
Extended single-cone anchor	791.6	744	106.4

Under the fatigue load, if the stress at certain position of the steel strands is too large, there will be an accumulation of fatigue damage, reducing the full utilization of the tensile properties of steel strands. In other words, the smaller the maximum Mises stress on the steel strands is, the more favorable it is for the full utilization of the tensile properties of the steel strands. According to the previous research [29-31] and the special requirements of the FAST engineering, when the maximum Mises stress is not greater than 110% of the tensile stress, the stress concentration of the steel strand is acceptable, otherwise, it is not acceptable. It can be seen from table 1 that the single-cone anchor does not meet the requirements. The stress on the steel strands in the double-cone anchor and the extended single-cone anchor gradually decreases along the opposite direction of Y axis, which meets the design requirements. However, the double-cone anchor has more advantages because of its smaller diameter, less material consumption and less gravity. The finite element analysis results also verify the correctness of the stress calculation results in 4.2.

4.4 Fabrication and Performance Verification of New Cable Anchor

Basically, cable anchor of all types share the same values of α and β. Therefore, α_1 is set at 4.1° according to regular cable anchor designing, and α_2 is set at 3°. The friction angle β is conservatively set at 5.7°[28]. r_1 should be set as small as possible to reduce the size and weight of the cable anchor while being big enough to accommodate the steel strands.

The cable series (S3, S5, etc., depending on the number of steel strands) should be designed with the same anchorage efficiency index m_A if they share the same double-cone cable anchor. According to Eq. (30), the following equation is obtained:

$$\frac{S}{Hr_w \tan(\alpha + \beta)} = \pi \frac{\dfrac{2}{m_A} - k_1}{k_3} \tag{40}$$

where r_w is the free end radius of the main anchor cup when $w=1$ or auxiliary anchor cup when $w=3$.

The same type cable anchors share approximately the same stress concentration coefficient; therefore,

$$C = \pi \frac{\dfrac{2}{m_A} - k_1}{k_3} \tag{41}$$

$$H = \frac{S}{Cr_w \tan(\alpha + \beta)} \tag{42}$$

Based on an integrated approach combining calculating and testing, the parameters of a certain design can be determined first, which can later be used to determine the constant C. Finally, the constant C will be introduced into Eq. (42) to calculate the anchorage length (H) of other types of cable.

The anchorage length (H_{S3J}) of the S3J-cable is determined as 225 mm; The main anchor cup length ($H_{1,S3J}$) = 106mm; The auxiliary anchor cup length ($H_{2,S3J}$) = 119mm; The cross-sectional area (S_{S3J}) = 478.9mm^2; The radius of free end ($r_{1,S3J}=r_{3,S3J}$) = 33mm. When the above parameters are brought into Eq. (42), the constant $C = 0.793$ can be obtained.

The typical S4J-cable of the FAST project was taken as an example, where $C = 0.793$; $\alpha_1=4.1°$; $\alpha_2 =3°$; $\beta=5.7°$; $r_{1,S4J}=r_{3,S4J}=40$mm; $S_{S4J}=618.9$mm^2. When the above parameters are brought into Eq. (42), the main anchor cup length ($H_{1,S4J}$) = 113mm; The auxiliary anchor cup length ($H_{2,S4J}$) = 127mm can be obtained. So the anchorage length (H_{S4J})=240mm.

According to Eq. (42), the anchorage length of other types of cable is shown in Table 2.

Table 2

Anchorage lengths of various cable models

Model	Number of steel strand(s)	Number of steel wires	Cross-sectional Area of cable S (mm²)	Radius of free end $r_1 = r_3$ (mm)	Main anchor cup length H_1 (mm)	Auxiliary anchor cup length H_2 (mm)	Anchorage length (mm)
S1J	1	3	198.9	25	58	65	123
S2J	2	3	338.9	32	77	87	164
S3J	3	3	478.9	33	106	119	225
S4J	4	3	618.9	40	113	127	240
S5J	5	3	758.9	42	132	148	280
S6J	6	3	898.9	45	146	164	310
S7J	7	3	1038.9	50	151	171	322
S8J	8	3	1178.9	55	156	176	332
S9J	9	3	1318.9	57	169	190	359

Note：Sz-cable and SzJ-cable use the same anchor, z is the number of steel strands.

The National Astronomical Observatory of China has proposed the requirements for cable fatigue test：1) For cables with stress amplitude greater than 450 MPa in service, the stress amplitude is taken as 500 MPa during fatigue test; 2) For cables with stress amplitude greater than 400MPa and less than 450MPa in service, the stress amplitude in fatigue test is 50MPa larger than that in service; 3) For cables with stress amplitude less than or equal to 400MPa in service, the stress amplitude in fatigue test is 450 MPa. The upper limit stress of the fatigue test is $0.4\sigma_b$ (where σ_b is the standard strength). Once a single steel wire is broken or the cable anchor is damaged, the test is considered as failure.

According to the above scheme, we made 9 cables for prototype fatigue test. The test scheme are shown in Table 3.

Table 3

Fatigue test results of cables

Group	Number	Cable type	Load (kN)	Stress amplitude (MPa)	Test cycles (×10,000)
1	1	S3	102.5~312.5	500	200
	2	S3	102.5~312.5	500	200
	3	S3	102.5~312.5	500	200
2	4	S6	204~624	500	100
	5	S6	204~624	500	100
	6	S6J	218.4~667.8	500	100
3	7	S4J	151.0~460.4	500	200
	8	S5J	192.7~564.6	490	200
	9	S6J	264.3~668.8	450	200

The cable body of S3-cable is composed of 3 steel strands with diameter of 15.4mm. Correspondingly, the cable body of S6-cable is composed of 6 steel strands, while the cable body of S6J-cable includes 3 steel wires besides 6 steel strands. In other words, "J" means that the cable body of this cable contains not only steel strands but also 3 steel wires. The cross sections of S6-cable and S6J-cable are shown in fig. 17.
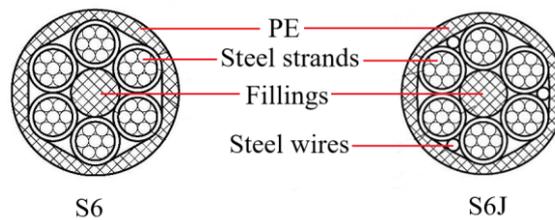
Fig. 17. Section of cable body

The effective sectional area of S6 type cable body is 840mm^2. The standard ultimate tensile force of the steel strands is 260kN, so the cable force limit of S6-cable is 1560kN. The upper limit load of fatigue test is 40% of the cable force limit = 624kN. When the stress amplitude is 500MPa, the corresponding lower limit load is 204kN.

The fatigue performance test is based on the "Technical Conditions of Cable-stayed Bridge Hot-extruded Polyethylene High-strength Steel Wire Cables"[32] and "Anchors, Clips and Connectors for Prestressed Tendons"[33]. The main test equipment is MTS universal test actuator. Before the fatigue test, the cable is pre-tensioned with 10% of the cable force limit, and then tensioned to 60% of the cable force limit to eliminate the Phase I slippage between the steel strands and the epoxy iron sand. The pressure is maintained for about 30 minutes. After holding pressure, unload to the lower limit load of the fatigue test and then the fatigue test is officially started. The stress amplitude is 500 MPa, and the frequency is 4 HZ. The test site of S6-cable is shown in Fig. 18.
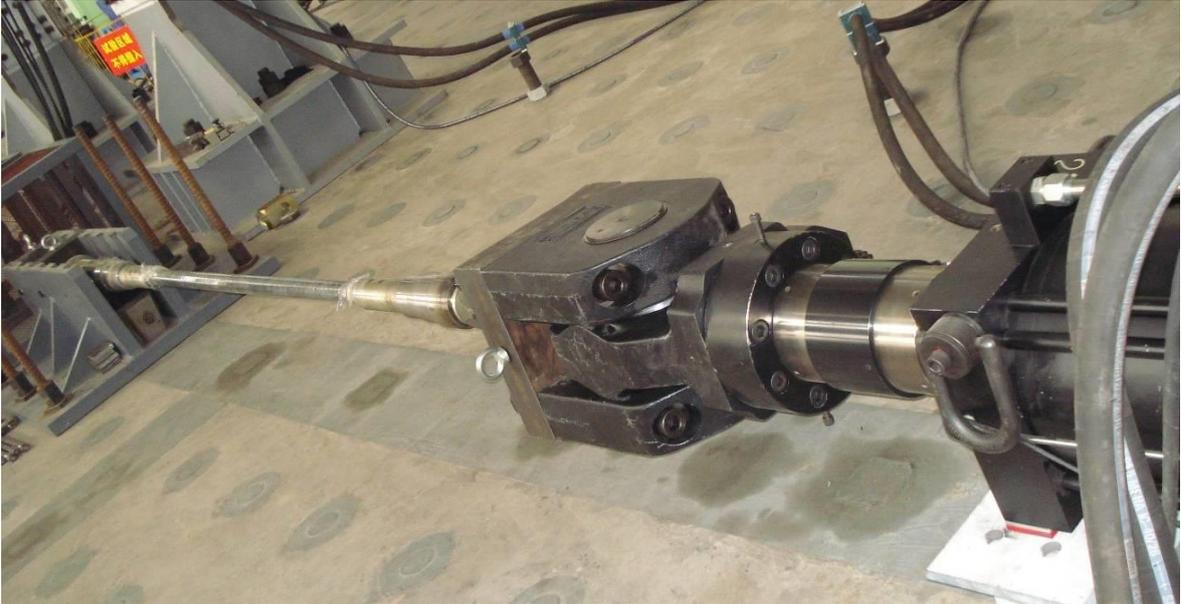
Fig. 18. Test site of S6-cable

After testing, the steel wire in the cable did not break, and the outer protective layer of the steel wire did not suffer fatigue damage, and the anchor head did not suffer fatigue damage. The results show that when the stress is 450-500MPa, all products meet the relevant requirements of fatigue performance. Moreover, in the fatigue test, the elastic modulus of the S3-cable were measured. As shown in Table 4, it was found that the elastic modulus of the cable was relatively stable throughout the test process, and the slight increase was due to the relaxation of the steel wire.

Table 4

Elastic modulus of S3-cable during fatigue test

Test cycles (×10,000)	Elastic modulus （MPa）		
	No.1	No.2	No.3
0	196.71	195.80	196.16
100	197.67	197.49	196.52
200	199.78	198.82	197.45

5. Conclusions

In this study, stress analyses are conducted on the cable anchor for FAST project, which combines the epoxy iron sand and steel strands following the theory of Elasticity. The following conclusions are reached:

1. The radial compressive stress distribution increases as the diameter of the inner conical hole decreases, which means the load end is where the stress concentration of the steel strands forms.

2. There is a clear mathematical connection involving the six parameters (anchorage efficiency index, stress concentration coefficients, cross-sectional area of steel strands, sum of   and   , R_1 and H).

3. The relationship between the anchorage efficiency coefficient and its influencing factors is also established.

4. The proposed innovative double-cone cable anchor consisting of a main anchor cup and an auxiliary anchor cup can effective in reducing the stress concentration at the load end.

5. A method for adjusting the initial stress of the cable anchor is proposed which effectively reduces the stress concentration of the steel strands inside the chilled cast anchor.

Increasing the number of cones can effectively reduce the stress concentration of the steel strands inside the chilled cast anchor. In order to improve the fatigue resistance of cable anchor，the number of cones can be increased to 3 or more.

Acknowledgments

Data Availability Statement

All data, models, and code generated or used during the study appear in the submitted article.

Appendix

The calculation diagram of thick-walled cylinder is shown in fig. 19.
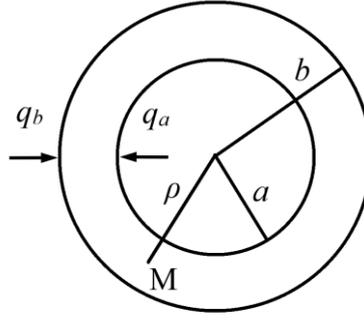
Fig. 19. Calculation diagram of thick-walled cylinder

According to the Lame's Equation，For point M，the stress solution of thick-walled cylinder is as follows.

$$\sigma_\rho = \frac{a^2 b^2 (q_b - q_a)}{b^2 - a^2}\frac{1}{\rho^2} + \frac{a^2 q_a - b^2 q_b}{b^2 - a^2}$$

$$\sigma_\varphi = -\frac{a^2 b^2 (q_b - q_a)}{b^2 - a^2}\frac{1}{\rho^2} + \frac{a^2 q_a - b^2 q_b}{b^2 - a^2}$$

(43)

The displacement solutions of thick-walled cylinders are shown as follows.

$$u_\rho = \frac{1}{E}\left[-(1+v)\frac{a^2 b^2 (q_b - q_a)}{b^2 - a^2} + (1-v)\frac{a^2 q_a - b^2 q_b}{b^2 - a^2}\rho\right]$$

(44)

For solid cylinders, in other words $a = 0$, $q_a = 0$, the stress solution is as follows.

$$\sigma_\rho = -q_b; \sigma_\varphi = -q_b$$

(45)

The displacement solution is as follows.

$$u_\rho = -\frac{1-v}{E}q_b\rho$$

(46)

For plane strain problems, the displacement is as follows.

$$u_\rho = -\frac{1-v-2v^2}{E}q_b\rho$$

(47)

Reference

[1] R. D. Nan, Five hundred meter aperture spherical radio telescope (fast). Science in China Series G, 49, 2, (2006), 129-148, http://doi.org/10.1007/s11433-006-0129-9.
[2] H. George, D. Shi, M. Richard N., K. Matthew, L. Ke-Jia, X. Ren-Xin, The role of fast in pulsar timing arrays. Physics, 19, 2, (2019), 397-424, http://doi.org/10.1088/1674-4527/19/2/20.
[3] R. D. Nan, Q. M. Wang, L. C. Zhu, W. B. Zhu, C. J. Jin, H. Q. Gan, Pulsar Observations with Radio Telescope FAST. Chinese Journal of Astronomy & Astrophysics, 6, S2, (2006), 304-310, http://doi.org/10.1088/1009-9271/6/S2/57.
[4] C. J. Jin, R. D. Nan, H. Q. Gan, The fast telescope and its possible contribution to high precision

astrometry. Proceedings of the International Astronomical Union, 3, S248, (2007), 178-181, http://doi.org/10.1017/S1743921308018978.

[5] P. Jiang, R. D. Nan, L. Qian, Y. L. Yue, System solutions study on the fatigue of the fast cable-net structure caused by form-changing operation. Research in Astronomy and Astrophysics, 15, (2015), 1758-1772, http://doi.org/10.1002/clc.4960071112.

[6] P. Jiang, Q. W. Li, R. D. Nan, Research on design of adaptive connecting mechanisms for the cable-net and panels of fast. Research in Astronomy and Astrophysics,,9, (2017), 121-130, http://doi.org/10.1088/1674-4527/17/9/99.

[7] R. D. Nan, G. X. Ren, W. B. Zhu, Y. J. Lu, Adaptive cable-mesh reflector for the fast. Acta Astronomica Sinica, 44, 2, (2003), 13-18 .

[8] Y. F. Luo, C. G. Deng, G. Q. Li, Y. M. He, Structural analysis of fast reflector supporting system. Astrophysics & Space Science, 278, 1-2, (2001), 231-236, http://doi.org/10.1023/A:1013131502739.

[9] H. L. Qian, F. Fan, S. Z. Shen, Q. M. Wang, Analysis on cable-net structure supporting the reflector of fast. Journal of Harbin Institute of Technology, 37, 6, (2005), 750-752, http://doi.org/10.1080/02726340590910084.

[10] Q. Heng, J. Cheng, An optimization of the shape of fast reflector panels. Research in Astronomy and Astrophysics, 10, 8, (2010), 797-804, http://doi.org/10.1088/1674-4527/10/8/009.

[11] P. Jiang, W. X. Zhu, F. Liu, Q. M. Wang, Y. L. Yue, L. Qian, et al. Fatigue performance evaluation of fast cable-net structures and development of a new type of steel cable system with high fatigue resistance. Engineering Mechanics, 32, 09, (2015), 243-249, http://doi.org/10.6052/j.issn.1000-4750.2014.03.0142.

[12] P. Jiang, R. D. Nan, L. Qian, Y. L. Yue, Studying solutions for the fatigue of the fast cable-net structure caused by the process of changing shape. Research in Astronomy and Astrophysics, 15, 10, (2015), 1758-1772, http://doi.org/10.1088/1674-4527/15/10/013.

[13] P. Jiang, Numerical investigation on fatigue problem of cable net structure of five-hundred-meter aperture spherical radio telescope. Advanced Materials Research, 936, (2014), 1351-1355, http://doi.org/10.4028/www.scientific.net/AMR.936.1351.

[14] P. Jiang, Deformation strategy optimization of FAST cable-net structure for fatigue problem. General Assembly & Scientific Symposium IEEE, (2014), http://doi.org/10.1109/URSIGASS.2014.6930003.

[15] Recommendations for Stay Cable Design, testing and installation. Post-tensioning institute (PTI) fifth edition, (2007).

[16] Fib bulletin 30, acceptance of stay cable systems using prestressing steels. International Federation for Structural Concrete, (2005).

[17] Cable stays-Recommendations of French inter-ministerial commission on Prestressing, SETRA, France, (2002).

[18] W. Xin, Z. Wu, W.Gang, Z. Hong, F. Zen, Enhancement of basalt FRP by hybridization for long-span cable-stayed bridge. Composites Part B, 44, 1, (2013), 184-192, http://doi.org/10.1016/j.compositesb.2012.06.001.

[19] R. Xiao, F. Liu, X. Zhang, Study of the fatigue problem of the side suspender of multi-span cable-stayed suspension bridge. Iabse Symposium Report, 102, 43, (2014), 123-128, http://doi.org/10.2749/222137814814027440.

[20] M. Zhao, J. Di, Fatigue load for cable-girder anchorage structure of highway and light-railway cable stayed bridge. Advanced Materials Research, 838-841, (2013), 1028-1033, http://doi.org/10.4028/www.scientific.net/AMR.838-841.1028.

[21] S. Y. Wang, J. D. Zhi, Research on heavy-load high fatigue stress amplitude cable and anchorage of cable-stayed bridge. Bridge Construction, 3, (2002), 14-16,

http://doi.org/10.3969/j.issn.1003-4722.2002.03.004.

[22] B. Feng, X. Wang, Z. S. Wu, Static and Fatigue Behavior of Multitendon CFRP Cables with Integrated Anchorages. Journal of Composites for Construction, 23, 6, (2019), http://doi.org/10.1061/(ASCE)CC.1943-5614.0000982.

[23] Z. G. Ping, Y. Yu, C. S. Cai, Z. H. Zhang, Y. Ding, Mechanical Behavior and Optimal Design Method for Innovative CFRP Cable Anchor. Journal of Composites for Construction, 23, 1, (2019), http://doi.org/10.1061/(ASCE)CC.1943-5614.0000900.

[24] N. A. M. Khairussaleh, G. A. R. Parke, M. Imam, Fatigue analysis of cable anchorages on cable-stayed bridges. Multi-Span Large Bridges - Proceedings of the International Conference on Multi-Span Large Bridges, (2015), 937-946, http://doi.org/10.1201/b18567-119.

[25] H. Qian, Y. Li, F. Feng, X. Jin, Q. Zeng, Experimental study of fatigue performance of cable in the FAST project. International Conference on Electric Technology & Civil Engineering, (2011), http://doi.org/10.1109/ICETCE.2011.5775843.

[26] K. Mei, S. Sun, L. Bo, Y. Sun, G. Jin, Experimental investigation on the mechanical properties of a bond-type anchor for carbon fiber reinforced polymer tendons. Composite Structures, 201, (2018), 193-199, http://doi.org/10.1016/j.compstruct.2018.05.153.

[27] Z. W. Deng, W. M. Leng, J. F. Zou, J. Tang, Calculation of pre-stress cable transference of load and effect of anchor. Journal of Central South University, 42, 2, (2011), 501-507, http://doi.org/10.3724/SP.J.1077.2011.00271.

[28] W. X. Zhu, R. H. Sang, L. Yang, H. Lei, Optimizing the anchoring structure for a super large cable-net structure with improved fatigue resistance. Advances in Structural Engineering, 23, (2019), http://doi.org/10.1177/1369433219878854.

[29] F. M. Li, X. Y. Luo, K. J. Wang, Y. S. Ji, Pitting Damage Characteristics on Prestressing Steel Strands by Combined Action of Fatigue Load and Chloride Corrosion. Journal of Bridge Engineering, 22, 7, (2017), http://doi.org/10.1061/(ASCE)BE.1943-5592.0001057.

[30] X. R. Yu, G. W. Yao, L. F. Gu, W. Q. Fan, Numerical and Experimental Study on the Steel Strands under the Coupling Effect of a Salt Spray Environment and Cyclic Loads. Materials, 13, 3, (2020), http://doi.org/10.3390/ma13030736.

[31] S. Nakamura, K. Suzumura, Experimental Study on Fatigue Strength of Corroded Bridge Wires. Journal of Bridge Engineering, 18, 3, (2013), 200-209, http://doi.org/10.1061/(ASCE)BE.1943-5592.0000366.

[32] Technical Conditions of Cable-stayed Bridge Hot-extruded Polyethylene High-strength Steel Wire Cables. GB／T18365-2001, (in chinese).

[33] Anchors, Clips and Connectors for Prestressed Tendons. GB/T 14370-2007, (in chinese).